TDA Progress Report 42-98

August 15, 1989

Performance Effects of Tie-Truss Modifications for a 70-Meter Centerline Beam Waveguide Antenna

J. J. Cucchissi
Ground Antennas and Facilities Engineering

The elevation-axis tie truss of the 70-m antennas would have to be modified to accommodate a centerline beam waveguide. To accomplish this, the center section of the tie truss has to be altered, causing a change in the tie-truss compliance and affecting structural performance. Even with the center section completely removed, the worst-case rms pathlength error due to gravity load is increased from 0.025 to only 0.030 inches. Using a simple postprocessor technique, the effects of modifying the compliance can be predicted without resorting to multiple and costly reanalyses of large finite-element models on a mainframe computer.

I. Introduction

With the imminent implementation of beam waveguide technology in the Deep Space Network, a study was initiated to predict the performance degradation due to retrofitting existing antennas in the 70-m subnet with a centerline or on-axis beam waveguide. Whereas the 70-m antenna structure was designed for a dish-mounted feedcone (Fig. 1) and no allowance made for an on-axis beam waveguide, some structural components of the main reflector and elevation wheel would obstruct the path of microwave energy of a beam waveguide system. The first significant obstruction is a 56-foot tie truss (Figs. 2 and 3). It is a space truss of triangular cross section that is integral with the reflector backup and elevation wheel substructures and that runs parallel to the elevation axis and connects the two elevation bearing castings. To allow a beam waveguide shroud to pass through this region, the center section would have to be modified or removed.

The purpose of this study was to determine the effect of tie-truss stiffness on the main reflector surface distortion under gravity load. Specifically, the analyses quantified the sensitivity of the gravity rms half-pathlength error to the stiffness of the tie-truss center section. Supplemental analyses also examined changes to the lower frequency modes when the center section is removed completely.

The sensitivity analyses described herein were performed using the methods of structural modification reanalysis [1, 2] and correlation analysis [2]. The specific procedures used are explained briefly; more rigorous descriptions of the theory and further applications can be found in the references.

II. Methodology

The 70-m tipping structure comprises the main reflector, elevation wheel, subreflector, and quadripod. A planar-symmetric finite-element half model of this structure includes 6,776 finite elements (primarily axial force bars), 1,994 nodes, and 5,982 translational degrees of freedom. Finite-element analysis and microwave-pathlength analysis is accomplished via the JPL-IDEAS finite-element analysis and design optimization program [3] on the UNIVAC. Sensitivity coefficients, derived from the large mainframe analysis model, are incorporated into PC-based postprocessing software that uses a combination of structural modification reanalysis and correlation analysis to assess the effect on performance when the cross-sectional areas of selected structural members are reduced or when the members are removed completely. Some postprocessor results were verified via mainframe finite-element processing.

The model was analyzed first for gravity load and the forces in the members in the central region of the tie truss were examined (Fig. 3). Those members that carried at least one percent of the gravity load and would obstruct a centerline beam waveguide path were selected for modification. For this study, nine bars were selected.

A. Structural Modification Reanalysis

To model the effects of modifying these selected members, sets of self-equilibrating unit virtual loading pairs [1], called indicator loads, are applied to the finite-element model at the terminal nodes of each of the members to be altered, one set per member. Static analysis is performed for each set separately and also for the y and z components of the gravity load. The JPL-IDEAS program provides: (1) the forces due to y and z gravity, and (2) the forces due to the indicator loadings, for each of the members to be altered. The following matrices then can be constructed:

$\mathbf{P_I}$ $2 \times N$ matrix of original forces for N altered members, z and y gravity rows

$\mathbf{P_S}$ $N \times N$ matrix of forces in N altered members for indicator loadings

$\mathbf{F}$ $N \times N$ diagonal matrix of original flexibilities of N altered members

$\mathbf{SF}$ $N \times N$ diagonal matrix of modified flexibilities of N altered members

Using the calculated member distortions

$$\mathbf{E_I} = \mathbf{F}\,\mathbf{P_I^T} \tag{1}$$

$$\mathbf{E_S} = \mathbf{F}\,\mathbf{P_S} \tag{2}$$

$$\mathbf{E_0} = \mathbf{SF} = \text{factor} * \mathbf{F} \tag{3}$$

and enforcing compatibility, the $N \times 2$ modifier matrix $\mathbf{R}$ is found by solving

$$(\mathbf{E_0} - \mathbf{E_S})\mathbf{R} = \mathbf{E_I} \tag{4}$$

A more detailed discussion of reanalysis is presented in [1].

B. Correlation Analysis

After determining the $\mathbf{R}$ modifier matrix, the gravity loading pathlength error analysis for the modified structure can proceed. The pathlength error vectors for z- and y-gravity loads after modification can be assembled from the independent pathlength error vectors for z and y gravity before modification and the indicator loads as follows:

$$\left[\vec{\rho}_z\ \vec{\rho}_y\right] = \left[\vec{\rho}_{z_0}\ \vec{\rho}_{y_0}\right] + \left[\vec{\rho}_1\ \vec{\rho}_2\ \ldots\ \vec{\rho}_N\right]\mathbf{R} \tag{5}$$

where $\vec{\rho}_k$ = best-fit pathlength error vector for load k and subscripts z_0, y_0 refer to z and y gravity response before modification, and 1,2,3,..., N refer to indicator loads.

At any elevation angle α, the gravity pathlength error vector is

$$\vec{\rho}_G = \left[\vec{\rho}_z\ \vec{\rho}_y\right]\mathbf{c} \tag{6}$$

where

$$\mathbf{c} = \begin{bmatrix} \zeta \\ \eta \end{bmatrix}$$

and $\zeta = \sin\gamma - \sin\alpha$, $\eta = \cos\gamma - \cos\alpha$, and γ = rigging angle (usually 45 deg), α = any elevation angle, $0 \leq \alpha \leq 90$ deg.

So, for the modified structure

$$\vec{\rho}_G = \left[\vec{\rho}_{z_0}\ \vec{\rho}_{y_0}\right]\mathbf{c} + \left[\vec{\rho}_1\ \vec{\rho}_2\ \cdots\ \vec{\rho}_N\right]\mathbf{R}\,\mathbf{c} \qquad (7)$$

Forming the sums of squares:

$$\begin{aligned} SS = \vec{\rho}_G^{\mathbf{T}}\vec{\rho}_G =& \mathbf{c}^{\mathbf{T}}\mathbf{P}_{G_0}^{\mathbf{T}}\mathbf{P}_{G_0}\mathbf{c} \\ &+ \mathbf{c}^{\mathbf{T}}\mathbf{P}_{G_0}^{\mathbf{T}}\mathbf{P}_N\mathbf{R}\,\mathbf{c} \\ &+ \mathbf{c}^{\mathbf{T}}\left(\mathbf{P}_{G_0}^{\mathbf{T}}\mathbf{P}_N\mathbf{R}\right)^T\mathbf{c} \\ &+ \mathbf{c}^{\mathbf{T}}\mathbf{R}^{\mathbf{T}}\mathbf{P}_N^{\mathbf{T}}\mathbf{P}_N\mathbf{R}\,\mathbf{c} \end{aligned} \qquad (8)$$

where $\mathbf{P}_{G_0} = [\vec{\rho}_{z_0}\ \vec{\rho}_{y_0}]$ and $\mathbf{P}_N = [\vec{\rho}_1\ \vec{\rho}_2\ \cdots\ \vec{\rho}_N]$.

Using the notation C_{ij} = correlation coefficient for pathlength error vectors $\vec{\rho}_i$ and $\vec{\rho}_j$, and RMS_k = the best-fit rms pathlength error for vector $\vec{\rho}_k$, and noting that $C_{ij} = \vec{\rho}_i^{\mathbf{T}}\,\vec{\rho}_j/(\mathbf{RMS}_i * \mathbf{RMS}_j)$, the first term in Eq. (8) can be shown to be:

$$A = \mathbf{c}^{\mathbf{T}}\,\mathbf{RM}_{zy}\,\mathbf{C}_{zy}\,\mathbf{RM}_{zy}\mathbf{c}$$

where

$$\mathbf{RM}_{zy} = \begin{bmatrix} RMS_z & 0 \\ 0 & RMS_y \end{bmatrix}$$

and

$$\mathbf{C}_{zy} = \begin{bmatrix} 1 & C_{zy} \\ C_{zy} & 1 \end{bmatrix}$$

the second and third terms can be shown to be:

$$B_1 = \mathbf{c}^{\mathbf{T}}\mathbf{RM}_{zy}\mathbf{C}_{GN}\mathbf{RM}_N\mathbf{R}\,c$$

$$B_2 = \mathbf{c}^{\mathbf{T}}\left(\mathbf{RM}_{zy}\mathbf{C}_{GN}\mathbf{RM}_N\mathbf{R}\right)^{\mathbf{T}}\mathbf{c}$$

where

$$\mathbf{C}_{GN} = \begin{bmatrix} C_{z1} & C_{z2} & \cdots & C_{zN} \\ C_{y1} & C_{y2} & \cdots & C_{yN} \end{bmatrix}$$

and

$$\mathbf{RM}_N = \begin{bmatrix} RMS_1 & \cdots & \cdots & 0 \\ \vdots & RMS_2 & & \\ \vdots & & \ddots & \\ 0 & \cdots & \cdots & RMS_N \end{bmatrix}$$

for N altered members (indicator loads), and the fourth term can be shown to be:

$$C = \mathbf{c}^{\mathbf{T}}\mathbf{R}^{\mathbf{T}}\mathbf{RM}_N\mathbf{C}_{IJ}\mathbf{RM}_N\mathbf{R}\,\mathbf{c}$$

where

$$\mathbf{C}_{IJ} = \begin{bmatrix} 1 & C_{12} & C_{13} & \cdots & C_{1N} \\ C_{12} & 1 & C_{23} & \cdots & C_{2N} \\ C_{13} & C_{23} & 1 & \cdots & C_{3N} \\ \vdots & & & \ddots & \\ C_{1N} & C_{2N} & C_{3N} & \cdots & 1 \end{bmatrix}$$

The first term is the contribution due to y-gravity and z-gravity loads and is assumed invariant. The second and third terms are the contributions of each indicator load correlated with both y- and z-gravity. The fourth term is the contribution of each indicator load correlated with the other indicator loads. Note that all but the first term require the modifier matrix $\mathbf{R}$ calculated earlier using structural modification reanalysis.

The JPL-IDEAS program provides the best-fit rms pathlength error (RMS_k) for each of the loads and the correlation coefficient (C_{ij}) for all pathlength-error vector pairs. By substituting in these values each term is readily calculated. Summing the four terms and taking the square root yields the gravity rms pathlength error for a particular modification of the N selected members.

$$rms = \left(SS\right)^{1/2} = \left(A + B1 + B2 + C\right)^{1/2} \qquad (9)$$

For other changes to the N selected members only a new $\mathbf{R}$ matrix need be calculated. Response over the antenna elevation range is computed by varying α from 0 to 90 deg.

III. Natural Frequency Analysis

Since the gravity rms pathlength error was not severely degraded by removing the center section of the tie truss, the normal modes were examined and compared before and after removal. Again, the JPL-IDEAS program was used to perform the natural frequency analyses. For a half-model structure, two stiffness matrix decompositions are required, one with symmetric and one with anti-symmetric boundary restraints, to recover all allowable modes for the full structure.

Instead of being rigidly fixed at the elevation bearings, the stand-alone tipping-structure model is connected to linear springs simulating the lateral flexibility of the alidade at the elevation bearing locations. This modeling provides a more realistic representation of the alidade and tipping structure interaction. Furthermore, since only half the structure is modeled, the alidade flexibility is represented by two springs, one for symmetric and one for anti-symmetric boundary conditions. Independent static analyses of the alidade were performed to determine the lateral flexibility of the alidade at the bearings. These compliances were then incorporated into the tipping-structure model for normal modes analysis.

IV. Numerical Results

The graph in Fig. 4 shows the change in the gravity rms pathlength error over the antenna elevation range for a series of bar-area reductions. Each rms achieves a maximum value at the extreme elevation angle of 0 deg; the rms is zero, by definition, at the prescribed rigging angle of 45 deg. There is little discernible difference in antenna performance between the original model and one where the tie-truss stiffness was reduced by 80 percent. Even with the center section removed, the worst case rms is 0.030 in.

The extreme values plotted in Fig. 1 are listed in Table 1 under combined gravity rms at 0 and 90 deg, for an antenna rigged at 45 deg. Also included are the rms values for a 1-g y-gravity load, a 1-g z-gravity load, and the correlation coefficient for these two loads. The equation that accompanies the table shows a simple way to calculate the combined gravity response from the y and z components. These results reflect only the effect of uniformly downsizing each of the nine selected bars in the tie-truss center section by a percentage of their original area. No allowance is made for the reduction in gravity load due to reducing member areas because the weight of these members represents only 0.5 percent of the total gravity (dead) load. Also, the solutions assume stiffness reduction only with no further optimization of the reflector backup or tie-truss structures to compensate for the rms increase.

When spot-checked with mainframe finite-element model analyses, the postprocessor made accurate predictions as the bar areas were reduced. As the areas approached zero, however, the predictions became unreliable; the $(\mathbf{E_O}-\mathbf{E_S})$ matrix became singular, correctly indicating unstable nodes in the finite-element model. To accurately analyze this case, the bars and any extraneous nodes had to be removed from the model, and a mainframe finite-element analysis was performed. Those results for the center section removed are tabulated as the 100-percent area-reduction case.

In Table 2 is a comparison of the lowest anti-symmetric modes, showing the effects of including accurate representations of the alidade compliance across the elevation bearings. The percentage of the total inertia about the y (roll) axis and z (yaw) axis contributed by each mode is listed in the table under effective modal inertia. The anti-symmetric modes above the first were changed moderately, as indicated by the frequency shifts and the redistribution of the effective modal inertias. However, the first anti-symmetric mode, which is essentially torsion of the quadripod at 1.28 Hz, was unchanged. This frequency is of particular importance because it is the lowest natural frequency of the 70-m antenna and, as such, is a critical performance constraint. To avoid excitation of the antenna modes, the lowest frequency must be outside the position loop bandwidth of the antenna drive servo system.

When expressed as a percentage of the total inertia about each axis, effective modal inertias provide general information about the mode shape. In the coordinate system used for the tipping structure model (see Fig. 1), a value for θ_x indicates a pitch mode, for θ_y a roll mode, and for θ_z a yaw mode. For example, in Table 3 anti-symmetric mode 2 after removal is a mixture of roll and yaw, representing 12.1 percent of the inertia about the y axis and 5.6 percent of the inertia about the z axis. Mode 3 is also a mixed mode, although predominantly yaw and representing 23.9 percent of the inertia about the z axis. Highly localized vibrations or modes with a small fraction of the rotational inertia, such as torsion of the quadripod, will appear as small values in these tables; examination of the

eigenvector is required to determine the character or mode shape of these vibrations.

Tables 3 and 4 compare the natural frequency performance of the antenna before and after the complete removal of the tie-truss center section. The analyses incorporated appropriate alidade springs with different symmetric and anti-symmetric mode properties. Both the anti-symmetric (antenna roll and yaw) and the symmetric (antenna pitch) modes were unaffected by the removal.

V. Summary

Analysis indicates that the center section of the elevation tie truss can be removed with a predicted degradation in gravity pathlength error of 0.005 in. rms. In addition, the removal does not compromise the natural frequency performance. In the model, an alternate load path through an adjacent structure must have been in effect to compensate for the tie-truss removal. Before any modification of the existing tie truss is recommended, this load path must be clearly defined and the integrity of the structural elements composing this path must be verified.

The postprocessor techniques used in the study simplified the analysis and provided accurate and reliable results when compared to the mainframe finite-element analyses. They are also inherently self-checking. When the predictions became unreliable, the postprocessor correctly indicated that an instability existed in the finite-element model.

References

[1] R. Levy, "A NASTRAN Postprocessor for Structural Modification Reanalysis," *NASA TM X-2378, Vol. II*, pp. 737–747, September 1971.

[2] R. Levy, "Reanalysis, Compatibility, and Correlation in Analysis of Modified Antenna Structures," *TDA Progress Report 42-97*, vol. January–March 1989, Jet Propulsion Laboratory, Pasadena, California, pp. 367–381, May 15, 1989.

[3] R. Levy and D. Strain, "JPL-IDEAS Iterative Design of Antenna Structures," Computer Program C-7282, submitted to *Cosmic*, November 1988.

Table 1. Stiffness reduction effects on RMS pathlength error

Area or stiffness reduction, percent	1-g y-gravity RMS, in. (cm)	1-g z-gravity RMS, in. (cm)	Correlation coefficient, C_{zy}	Combined gravity[a] RMS, in. (cm)	
				EL 0 deg	EL 90 deg
0	0.0274 (0.0696)	0.0354 (0.0899)	0.1095	0.0254 (0.0645)	0.0210 (0.0533)
20	0.0275 (0.0699)	0.0356 (0.0904)	0.1146	0.0255 (0.0648)	0.0210 (0.0533)
40	0.0276 (0.0701)	0.0359 (0.0912)	0.1214	0.0257 (0.0653)	0.0210 (0.0533)
60	0.0281 (0.0714)	0.0365 (0.0927)	0.1303	0.0260 (0.0660)	0.0213 (0.0541)
80	0.0292 (0.0742)	0.0375 (0.0953)	0.1404	0.0267 (0.0678)	0.0220 (0.0559)
100	0.0315 (0.0800)	0.0412 (0.1046)	0.1291	0.0294 (0.0747)	0.0239 (0.0607)

[a] $RMS_\alpha = \left(\eta^2 RMS_y^2 + \zeta^2 RMS_z^2 + 2\eta\zeta RMS_y RMS_z C_{zy}\right)^{1/2}$

for $\alpha = 0$ deg, $\gamma = 45$ deg

$\eta = -0.2929$

$\zeta = 0.7071$

and for $\alpha = 90$ deg, $\gamma = 45$ deg

$\eta = 0.7071$

$\zeta = -0.2929$

Table 2. Comparison of anti-symmetric modes with and without simulated alidade compliance

Mode	With alidade compliance			Without alidade compliance		
	Frequency, Hz	Effective modal inertia, percent of total		Frequency, Hz	Effective modal inertia, percent of total	
		θ_y	θ_z		θ_y	θ_z
1	1.281	–	1.1	1.281	–	1.0
2	1.489	12.1	5.6	1.594	24.8	2.7
3	1.719	13.8	23.9	1.769	2.2	60.8

Table 3. Comparison of anti-symmetric modes before and after removal of tie-truss center section

Mode	Before removal			After removal			Mode shape
	Frequency, Hz	Effective modal inertia, percent of total θ_y	θ_z	Frequency, Hz	Effective modal inertia, percent of total θ_y	θ_z	
1	1.281	–	1.0	1.281	–	1.1	Yaw (Quad Torsion)
2	1.491	12.7	4.5	1.489	12.1	5.6	Roll + Yaw
3	1.736	13.0	21.5	1.719	13.8	23.9	Yaw + Roll

Table 4. Comparison of symmetric modes before and after removal of tie-truss center section

Mode	Before removal		After removal		Mode shape
	Frequency, Hz	Effective modal inertia, percent of total θ_x	Frequency, Hz	Effective modal inertia, percent of total θ_x	
1	2.389	41.6	2.381	42.4	Pitch
2	2.853	10.9	2.847	10.5	Pitch
3	3.262	2.3	3.255	2.1	Pitch

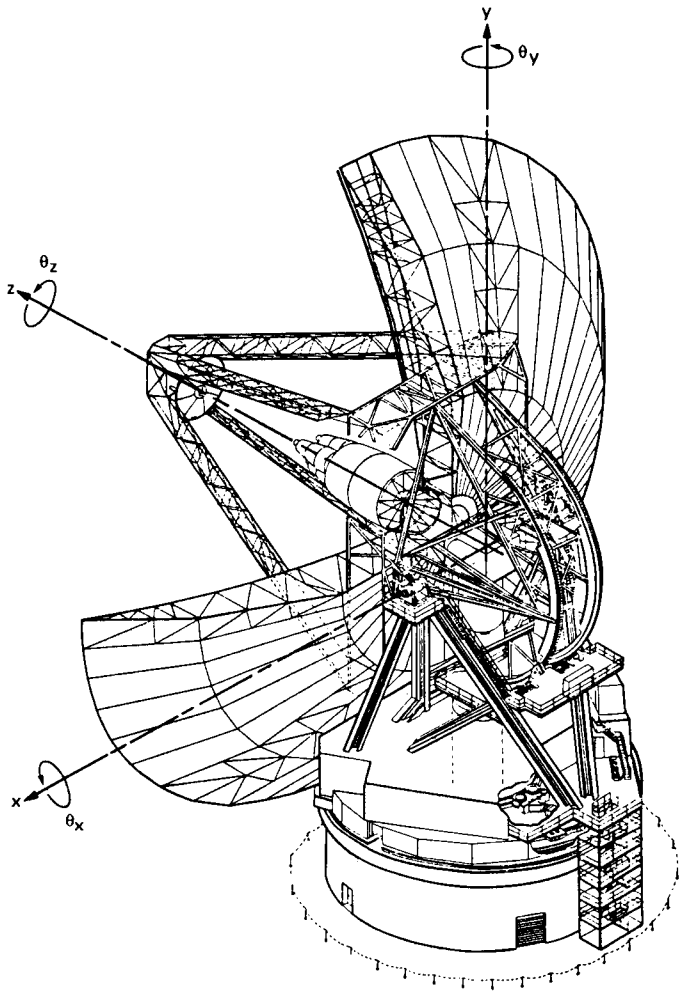

Fig. 1. Isometric view of the 70-m antenna showing coordinate system of the tipping structure.

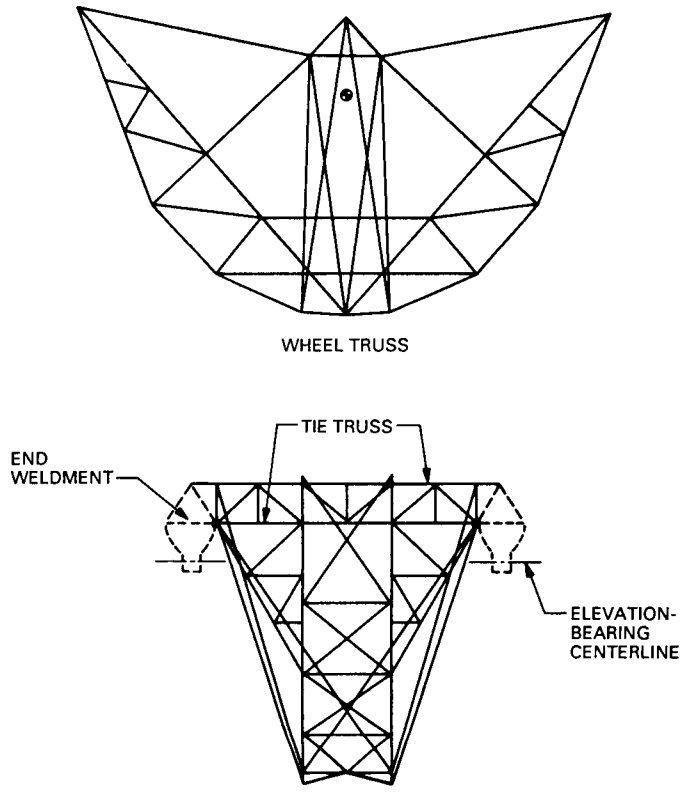

Fig. 2. 70-m antenna elevation wheel with tie truss.

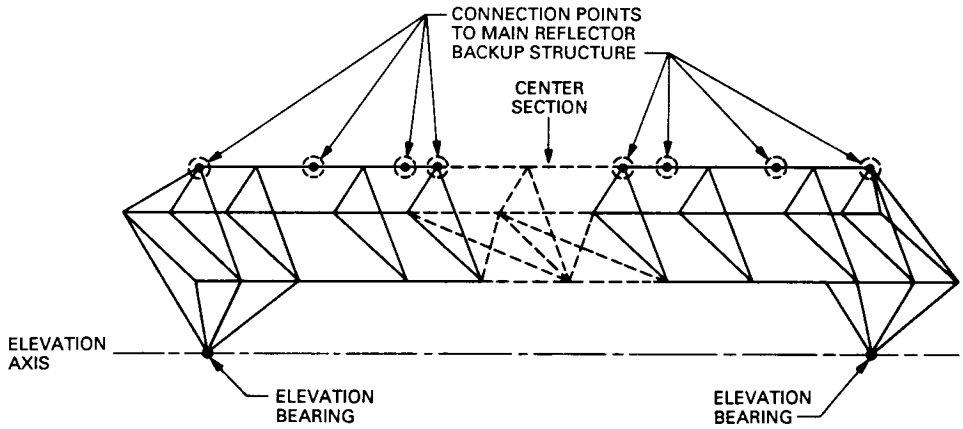

Fig. 3. Simplified view of tie truss showing region to be modified.

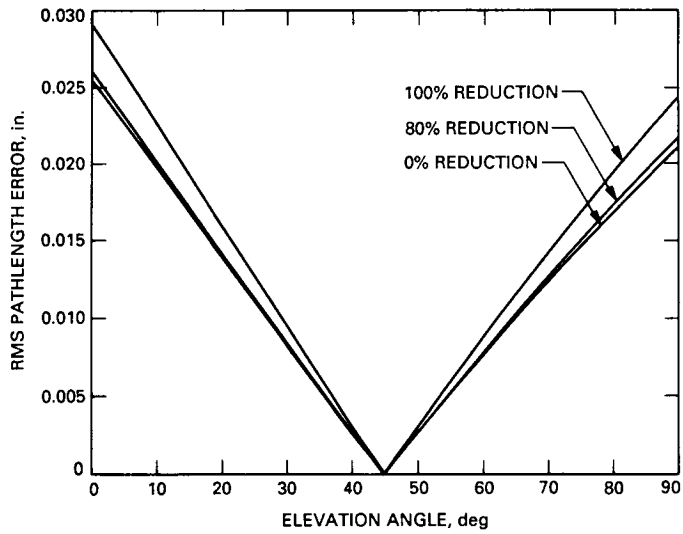

Fig. 4. Gravity RMS pathlength error for a series of bar-area (stiffness) reductions.